Interfacial Orientation of *Thermomyces lanuginosa* Lipase on Phospholipid Vesicles Investigated by Electron Spin Resonance Relaxation Spectroscopy†

Eva M. K. Hedin,‡ Pernille Høyrup,§ Shamkant A. Patkar,|| Jesper Vind,|| Allan Svendsen,|| Linda Fransson,‡ and Karl Hult*,‡

Department of Biotechnology, Royal Institute of Technology, Stockholm Center for Physics, Astronomy, and Biotechnology, SE-106 91 Stockholm, Sweden, Department of Chemistry, Building 207, Technical University of Denmark, DK-2800 Kgs. Lyngby, Denmark, and Novozymes A/S, Smørmosevej 25, DK-2880 Bagsvaerd, Denmark

Received February 22, 2002; Revised Manuscript Received July 10, 2002

ABSTRACT: The binding orientation of the interfacially activated *Thermomyces lanuginosa* lipase (TLL, EC 3.1.1.3) on phospholipid vesicles was investigated using site-directed spin labeling and electron spin resonance (ESR) relaxation spectroscopy. Eleven TLL single-cysteine mutants, each with the mutation positioned at the surface of the enzyme, were selectively spin labeled with the nitroxide reagent (1-oxyl-2,2,5,5-tetramethyl-Δ^3-pyrroline-3-methyl) methanethiosulfonate. These were studied together with small unilamellar vesicles (SUV) consisting of 1-palmitoyl-2-oleoyl-*sn*-glycero-3-phosphatidylglycerol (POPG), to which TLL has previously been shown to bind in a catalytically active form [Cajal, Y., et al. (2000) *Biochemistry 39*, 413−423]. The orientation of TLL with respect to the lipid membrane was investigated using a water-soluble spin relaxation agent, chromium(III) oxalate (Crox), and a recently developed ESR relaxation technique [Lin, Y., et al. (1998) *Science 279*, 1925−1929], here modified to low microwave amplitude (<0.36 G). The exposure to Crox for the spin label at the different positions on the surface of TLL was determined in the absence and presence of vesicles. The spin label at positions Gly61-Cys and Thr267-Cys, closest to the active site nucleophile Ser146 of the positions analyzed, displayed the lowest exposure factors to the membrane-impermeable spin relaxant, indicating the proximity to the vesicle surface. As an independent technique, fluorescence spectroscopy was employed to measure fluorescence quenching of dansyl-labeled POPG vesicles as exerted by the protein-bound spin labels. The resulting Stern−Volmer quenching constants showed excellent agreement with the ESR exposure factors. An interfacial orientation of TLL is proposed on the basis of the obtained results.

Lipases, classified in the group of triacylglyceride ester hydrolases (EC 3.1.1.3), are enzymes that hydrolyze triglycerides to di- and monoglycerides, glycerol, and free fatty acids. The lipases represent one of the most important enzyme classes employed in industry, in terms of both economic value and variety of use. Biotransformations of fats and oils, synthesis of surfactants and flavors, regioselective acylation, resolution of racemic compounds, and use in laundry detergents and the tanning and paper industries are areas in which lipases have found or are expected to find commercial application (*1*−*7*). A wide variety of lipase preparations with different catalytic properties are commercially available, which reflects the importance of these enzymes.

A distinguishing feature of lipases is that their hydrolytic activity, which is low on monomeric substrates, increases dramatically in the presence of an interface, such as a lipid−water interface. This phenomenon, which deviates from classical Michaelis−Menten kinetics, is known as interfacial activation [originally defined by Sarda and Desnuelle (*8*)] and has been observed in lipases of different origin, including microbial lipases. Organic solvents and detergents (at concentrations greater than their cmc[1]) are also known to induce this activation (*9*, *10*).

The crystal structures of several lipases have been reported (*11*−*16*), some of which have been complexed with inhibitors or cocrystallized with micelles (*17*−*21*). Despite a significant diversity in the amino acid sequence of lipases, the crystallographic data have revealed that their secondary and tertiary structures are quite well conserved (reviewed in refs *22*−*25*). All lipases exhibit the α/β hydrolase fold,

† This work was supported by the European Commission (Contract BIO4-CT972365).

* To whom correspondence should be addressed. Phone: +46 8 5537 8364. Fax: +46 8 5537 8468. E-mail: kalle@biochem.kth.se.

‡ Royal Institute of Technology.

§ Technical University of Denmark.

|| Novozymes A/S.

[1] Abbreviations: cmc, critical micellar concentration; Crox, chromium(III) oxalate; CW, continuous wave; dansyl DHPE, *N*-(5-dimethylaminonaphthalene-1-sulfonyl)-1,2-dihexadecanoyl-*sn*-glycero-3-phosphatidylethanolamine triethylammonium salt; DTT, DL-dithiothreitol; EDTA, ethylenediaminetetraacetic acid; ESR, electron spin resonance; FRET, fluorescence resonance energy transfer; HEPES, *N*-(2-hydroxyethyl)piperazine-*N*′-2-ethanesulfonic acid; Tris, tris(hydroxymethyl)aminomethane; K_{SV}, Stern−Volmer quenching constant; MS, mass spectrometry; MTSL, (1-oxyl-2,2,5,5-tetramethyl-Δ^3-pyrroline-3-methyl) methanethiosulfonate; MLV, multilamellar vesicles; NBD, 7-nitrobenz-2-oxa-1,3-diazol-4-yl; POPG, 1-palmitoyl-2-oleoyl-*sn*-glycero-3-phosphatidylglycerol; Rh, rhodamine; SDS, sodium dodecyl sulfate; SDSL, site-directed spin labeling; SL, spin labeled; SUV, small unilamellar vesicles; TLL, *Thermomyces lanuginosa* lipase; SL-TLL (and TLL-SL), spin-labeled *T. lanuginosa* lipase.

10.1021/bi020158r CCC: $22.00
Published on Web 11/07/2002

composed of a core of five or more parallel β-strands surrounded by a number of α-helices (*26*). In addition, the catalytic residues are found in the highly conserved Ser-His-Asp (Glu) triad.

Another important attribute for the majority of lipases is the existence of a "lid", usually a short α-helix or loop that covers the active site in the closed (inactive) conformation of lipases, which is the predominant conformation in aqueous solution in the absence of an interface. It is thought that the lid is displaced upon activation, thereby rendering access to the active site and exposing a large hydrophobic patch that facilitates association to a lipid surface (*27*, *28*). The closed and the open lipase conformations found in the crystal structures are believed to represent the start and the end of the interfacial activation pathway, where the lid movement plays a key role in the activation process (*28*, *29*). This process presumably consists of several steps, for which the mechanisms of activation and intermediate forms are still poorly understood. The X-ray data provide important, but predominantly static, information on protein structure. However, by employing spectroscopic biophysical methods, the dynamic properties of proteins can be monitored under physiologically relevant conditions.

An extensive spectroscopic study on *Thermomyces* (formerly *Humicola*) *lanuginosa* lipase (TLL) was recently reported, showing that TLL binds to small unilamellar vesicles (SUV) consisting of the phospholipid 1-palmitoyl-2-oleoyl-*sn*-glycero-3-phosphatidylglycerol (POPG) in a catalytically active conformation with the lid open and partially buried into the lipid bilayer (*30*). This 33 kDa, 269 amino acid, fungal lipase displays classical properties of interfacial activation (*31*). The crystal structures of TLL in both the closed and the open conformation have been solved (*16*, *20*). Recently, five new crystal structures of TLL were presented as obtained through systematic crystallographic studies, which provided new insights into the mechanisms in the interfacial activation pathway (*32*).

In the present paper, we have studied the binding orientation of TLL at the lipid−water interface of small unilamellar POPG vesicles, employing electron spin resonance (ESR) relaxation spectroscopy in combination with site-directed spin labeling (SDSL) on 11 TLL single-cysteine mutants. The technique of SDSL has during the past decade emerged as a powerful tool for studying protein structure and dynamics (reviewed in ref *33*). Employment of spin relaxation agents, such as chromium(III) oxalate (Crox) and molecular oxygen, in biological studies has afforded detailed structural and dynamic information for a diversity of proteins (for example, refs *34*−*38*). In the present study, we have used an ESR relaxation technique modified to low microwave amplitude ($<$0.36 G), which is applicable also on standard, commercial ESR equipment. In addition, we have compared this low-field method with the established method of progressive power saturation (*36*, *39*). The TLL orientation study has been further complemented by employing fluorescence spectroscopy, measuring the intermolecular quenching of dansyl-labeled POPG vesicles as exerted by the protein-bound spin labels. On the basis of the obtained data, a model for the interfacial orientation of TLL on POPG SUV is proposed, which is in good agreement with the existing structural and biophysical data on TLL.

MATERIALS AND METHODS

General. The spin-labeling reagent MTSL was purchased from Toronto Research Chemicals Inc. (Ontario, Canada) and POPG from Avanti Polar Lipids (Birmingham, AL). The lipid fluorophore *N*-(5-dimethylaminonaphthalene-1-sulfonyl)-1,2-dihexadecanoyl-*sn*-glycero-3-phosphatidylethanolamine triethylammonium salt (dansyl DHPE) was purchased from Molecular Probes Europe BV (Leiden, The Netherlands). Crox was synthesized by the method of Bailar and Jones (*40*). PD-10 desalting columns were purchased from Amersham Pharmacia Biotech (Uppsala, Sweden) and Slide-A-Lyzer dialysis cassettes (10 kDa molecular mass cutoff) from Pierce (Boule Nordic AB, Huddinge, Sweden).

Lipase Variants. The gene encoding *T. lanuginosa* lipase was cloned, sequenced, expressed, and purified as described previously (*7*, *41*). Specifically, 11 single-cysteine TLL mutants were produced in which a cysteine was introduced on the surface of the enzyme at the following positions: P42C (proline 42 exchanged for cysteine), G61C, K74C, D96C, T123C, D137C, T192C, R209C, T231C, I252C, and T267C. The presence of a cysteine at the correct position in each mutant was verified by gene sequencing. Protein concentration was determined from the absorbance at 280 nm using an extinction coefficient of 3.59×10^4 cm^{-1} M^{-1} based on amino acid composition (*42*).

Vesicle Preparation and Characterization. Vesicles containing POPG, or POPG with dansyl DHPE, 99:1 (mol/mol), were prepared as follows. Weighed amounts of the lipids were dissolved in chloroform/methanol, 1:1 (v/v). The organic solvent was evaporated under a weak stream of nitrogen, and the samples were kept under vacuum overnight. Multilamellar vesicles (MLV) were formed by adding buffer to the dried lipid film. Hydration and formation of the MLV lipid mixtures were performed at 55 °C for at least 30 min. SUV with a diameter of 50 nm were formed by extrusion twice through two stacked 100 nm size polycarbonate filters and 10 times through two stacked 50 nm size polycarbonate filters. The size distribution of the vesicles was analyzed by dynamic light scattering using a Malvern Zetasizer (Malvern Instruments Ltd., Malvern, U.K.).

Site-Specific Spin Labeling and Characterization of TLL Mutants. Titration of the TLL single-cysteine mutants with Ellman's reagent (*43*) indicated that the sulfhydryl group of the introduced cysteine was blocked, and electrospray MS revealed that it was disulfide linked to free cysteine [presumably during fermentation or purification (*44*, *45*)]. The surface-exposed cysteine was selectively reduced by treating the protein (1 mg/mL in 50 mM Tris−acetate, 2 mM EDTA, pH 7.7) with 0.3 mM DTT (from a freshly prepared stock solution) for 1 h at room temperature using the wild-type enzyme as a control. The DTT was removed by 2×90 min dialysis against the aforementioned buffer under an atmosphere of nitrogen. The protein was immediately treated with 45 molar equiv of the spin-labeling reagent MTSL (Chart 1) from a freshly prepared stock solution in ethanol. The final content of ethanol in the reaction mixture was 1.5% (v/v), and the MTSL remained totally soluble under these conditions. After 1 h the reaction mixture was subjected to gel filtration on a PD-10 column preequilibrated with 20 mM Na-HEPES, pH 7.0, and was further purified by extensive dialysis against the same buffer at 4 °C. The degree of spin-

Chart 1: (1-Oxyl-2,2,5,5-tetramethyl-Δ^3-pyrroline-3-methyl) methanethiosulfonate (MTSL)

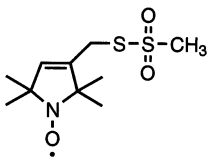

label incorporation was analyzed by continuous wave (CW) ESR spectroscopy against MTSL standard solutions and was found to range between 10% and 100% (mole percent) for the different mutants. Only insignificant amounts of MTSL (~1%) were detected in the wild-type enzyme, indicating that the three internal disulfide bridges stayed intact during the reaction. The spin-labeled enzymes were stored as aliquots at −20 °C and were stable for several months.[2] The specific hydrolytic activity was measured with a pH stat [employing a modification of the method described by Svendsen et al. (*7*)] on an emulsion of glyceryl tributanoate, where one lipase unit is defined as 1 μmol of released titratable acid per minute. The assay was performed at pH 7 and 25 °C on a sonicated (Branson sonifier W-250; 10 W during 1 min for 30 mL of substrate) 16 mM emulsion of glyceryl tributanoate (0.5% w/v) in a 2% (w/v) aqueous solution of gum arabicum and 0.2 M $CaCl_2$. Typically, 10 μL of enzyme (1 μM) was added to the 1.5 mL stirred emulsion, and the activity was monitored using an ABU91 Autoburet together with a TIM900 Titralab station and the software TimTalk 9, v1.4 (Radiometer, Copenhagen, Denmark).

ESR Spectroscopy. The ESR spectra were recorded on a Bruker (Rheinstetten, Germany) EMX EPR spectrometer with a 12 kW 10 in. magnet in the X-band at 9.75 GHz using a Bruker ER 4102 ST standard resonator for the subsaturating measurements with a microwave amplitude, h_1, less than 0.36 G. A Bruker ER 4117D-R dielectric resonator was used for the power saturation measurements with h_1 ranging between 0.02 and 1.6 G. The conversion efficiency factor, α, was estimated to 1 and 4 G/W$^{1/2}$ for the standard and the dielectric resonators, respectively. The spectra were recorded at room temperature using a 1 G, 100 kHz magnetic field modulation for phase-sensitive detection. A field modulation of 1 G ensures a well-defined signal, and the line broadening due to overmodulation is less than 10% (*46*). All measurements were performed under critical coupling conditions, and the spectra were recorded several times and summed for improvement of signal-to-noise ratio.

CW ESR Power Saturation Measurements. The effect of Crox on spin relaxation was analyzed on the spin-labeled TLL mutant I252C (I252C-SL) using the dielectric resonator. A stock solution of Crox (0.5 M) was prepared in 20 mM Na-HEPES, pH 7.0. A series of samples containing I252C-SL (23 μM) with increasing concentrations of Crox (0, 1.25, 2.50, 4.95, and 9.80 mM) was prepared in the same buffer. The samples (20 μL) were transferred into a quartz tube with an inner diameter of 0.5 mm, and ESR spectra were recorded at room temperature with the microwave power ranging from 0.02 to 160 mW in order to obtain the full power-saturation rollover curves.

[2] After approximately 6 months a notable decrease in the binding and the hydrolytic activity of the spin-labeled enzymes was observed.

CW ESR Low-Amplitude Measurements. Subsaturating, low-field ESR spectra were recorded on all spin-labeled TLL mutants at room temperature using the standard resonator and a microwave power up to 127 mW (h_1 < 0.36 G). Quartz tubes with an inner diameter of 1 mm were used, and the sample size was 50 μL. The spectra were recorded for the spin-labeled enzymes (15 μM in 20 mM Na-HEPES, pH 7.0) in the absence and presence of extruded, 50 nm POPG vesicles (3 mM POPG), after which Crox was added (to a final concentration of 9.8 mM) and the samples were analyzed again. The ESR signal intensity of the Crox-containing samples was corrected for dilution effects.

Fluorescence Quenching Experiments. The intermolecular quenching of dansyl fluorescence was analyzed on dansyl-labeled POPG vesicles together with the spin-labeled TLL's, in which the spin label acts as a quencher (*47*, *48*). The lipid fluorophore used, dansyl DHPE, has the dansyl positioned near the lipid headgroup. The experiments were carried out in 20 mM Na-HEPES at pH 7.0 and 25 °C. Unlabeled (reference) or spin-labeled TLL mutants were titrated to a 1 mM suspension of 50 nm lipid vesicles consisting of POPG/dansyl DHPE, 99:1 (mol/mol), and the fluorescence was monitored at 500 nm upon excitation at 350 nm using a SLM DMX-1100 spectrofluorometer (SLM Instruments Inc., Urbana, IL). The final concentration of lipase was less than 10 μM. The data was analyzed in accordance with the Stern−Volmer equation for collisional quenching:

$$F_0/F = 1 + K_{SV}[Q]$$

where F_0 and F are the intensities of fluorescence in the absence and presence of the quencher, respectively, [Q] is the molar concentration of quencher, and K_{SV} is the Stern−Volmer quenching constant.

ESR Theory and Data Analysis. (i) Progressive Power Saturation. Haas, Mailer and Robinson have established a method in which experimental ESR power saturation data is fit to an equation by which also non-Lorentzian line shapes can be accommodated (*36*, *39*). Accordingly, the power dependence of the peak to peak height of the central line in the first derivative ESR spectrum, ΔY, is given by

$$\Delta Y = \frac{cP_0^{1/2}}{(1 + P_0/P_2)^{\epsilon}} \quad (1)$$

where the prefactor c is related to the spin−spin relaxation time as $c = c'T_{2e}^2$, P_0 is the microwave power incident on the sample, ϵ is an adjustable line shape parameter, and P_2 is a saturation parameter (in units of watts). The microwave amplitude (in gauss), h_1, incident on the sample is dependent on the conversion efficiency factor of the resonator, α, as $h_1 = \alpha P_0^{1/2}$. The saturation parameter is defined as $P_2 = [(\gamma_e\alpha)^2 T_{1e}T_{2e}]^{-1}$ and is furthermore proportional to the product of the two relaxation rates:

$$P_2 \propto R_1R_2 \quad (2)$$

where the relaxation rates, given in units of field (gauss), are related by the electron gyromagnetic ratio, γ_e, to the spin−lattice and the spin−spin relaxation times through $R_1 = (\gamma_e T_{1e})^{-1}$ and $R_2 = (\gamma_e T_{2e})^{-1}$, respectively (*36*, *39*). P_2 defines the maximum of the power saturation rollover curve

together with the adjustable line shape parameter, ϵ (*36*, *39*), as $P_{max} = P_2/(2\epsilon - 1)$.

A spin relaxation agent, such as Crox, changes the relaxivity of a spin probe in a concentration-dependent manner through a Heisenberg exchange by collision between the two paramagnetic molecules (*49*, *50*):

$$R_1 = R_1^0 + \chi[\text{Crox}] \quad (3)$$

$$R_2 = R_2^0 + \chi[\text{Crox}] \quad (4)$$

where χ is the relaxivity of Crox and the superscript zero refers to the absence of Crox. The changes in P_2 upon addition of Crox are approximately proportional to the concentration of Crox in the vicinity of the spin probe (*36*):

$$\Delta P_2 = P_2 - P_2^0 \propto \chi(R_1^0 + R_2^0)[\text{Crox}] \quad (5)$$

Values of P_2 and ϵ are readily obtained by nonlinear least-squares regression analysis of the data points to eq 1 after the power saturation rollover curves have been established.

(ii) The Low-Field Method. At low incident microwave power, the denominator in eq 1 approaches unity (*39*), and it is seen that the signal intensity becomes approximately proportional to the incident microwave power:

$$\Delta Y \approx cP_0^{1/2} = c'\frac{1}{(R_2\gamma_e)^2}P_0^{1/2} \quad (1a)$$

Thus, for low incident power, the linear dependence of ΔY on the square root of the incident power is given by the proportionality constant $c = c'(R_2\gamma_e)^{-2}$. Furthermore, in analogy to eq 5, the change in the inverse square root of this slope, c, upon addition of Crox is found to be proportional to the local Crox concentration:

$$\Delta c^{-1/2} = \Delta\frac{1}{\sqrt{c}} = \frac{R_2\gamma_e}{\sqrt{c'}} - \frac{R_2^0\gamma_e}{\sqrt{c'}} = \frac{\gamma_e}{\sqrt{c'}}\chi[\text{Crox}] \quad (6)$$

The proportionality constants are readily available in the low (linear) power region of the power saturation rollover curves. However, for the orientation study performed in the present paper, the slopes were extracted by a linear least-squares fit to eq 1a of subsaturating ESR data obtained at low microwave amplitude ($h_1 < 0.36$ G), using a standard resonator.

(iii) Calculation of Exposure Factors. The exposure factor, Φ, is a measure of the exposure to a water-soluble spin relaxation agent for a nitroxide on the surface of an interfacially bound protein (*36*). In the present paper, the original expression for Φ was modified for using the ESR low-field parameters presented above. Accordingly, the differences in the inverse square root of the proportionality constant (the slope), $\Delta c^{-1/2}$, determine the relative exposure to Crox for the protein-bound nitroxides:

$$\Phi = \frac{(\Delta c^{-1/2})_{+\text{membrane}}}{(\Delta c^{-1/2})_{-\text{membrane}}} = \frac{[\text{Crox}]^{\text{local}}_{+\text{membrane}}}{[\text{Crox}]^{\text{local}}_{-\text{membrane}}} \quad (7)$$

where the superscript "local" refers to the effective Crox concentration at the spin probe moiety, and the presence of a lipid membrane reduces this concentration.

(iv) Calculation of Electrostatic Potential-Modulated Crox Concentrations and Regression Analysis of TLL−Membrane Orientation. The electrostatic potential of the POPG vesicle surface is highly negative, which reduces the concentration of anions in solution close to the membrane in relation to their bulk concentrations. The Boltzmann equation expresses the Crox concentration as a function of the electrostatic potential induced by the membrane (*36*):

$$C_{\text{Crox}}(r) = C_{\text{Crox}}(r = \infty)\exp\left(\frac{-z_{\text{Crox}}F\Psi(r)}{RT}\right) \quad (8)$$

where $C_{\text{Crox}}(r)$ is the molar concentration of Crox at a distance r normal from the membrane, z_{Crox} is the charge on Crox, $\Psi(r)$ is the electrostatic potential, F is the Faraday constant, R is the universal gas constant, and T is the absolute temperature. The electrostatic potential for a planar membrane of uniform charge density is described by the Poisson−Boltzmann equation (*36*, *51*), of which a second-order Tailor expansion allows an estimation of the electrostatic potential as

$$\Psi(r) = \Psi(0)\exp(-r/r_D) \quad (9)$$

where r_D is the Debye length (calculated to 8 Å for our system). The Debye length describes the variation of excess charge density with distance from a central ion in solution (*51*), and is dependent on the solution's ionic strength. A value of $\Psi(0) = 77$ mV [as previously determined experimentally for a similar system (*36*)] was used in the calculations. The Crox concentration can be calculated as a function of distance from the POPG membrane, and theoretical exposure factors Φ (r) can be calculated by

$$\Phi(r) = C_{\text{Crox}}(r)/C_{\text{Crox}}(\infty) \quad (10)$$

A regression analysis of the TLL−membrane orientation was performed by varying the distance between TLL and the membrane surface, and the two angles for rotation of TLL around its center. The theoretical exposure factors $\Phi(r)$ were compared with the experimental Φ values in order to obtain the normal distance of each spin label to the membrane. The atomic coordinates were extracted from the TLL X-ray structure [provided by Lawson et al. (*20*)] and used together with the obtained distances in the minimization trials (*36*). No attempt was made to model the nitroxides into the structure due to the uncertainty of position for the rather freely moving spin labels (as indicated by the ESR spectra). Instead, the sulfur atom of each cysteine side chain was used as a point of reference. The spin labels at positions D137C, T231C, and I252C were not included in the analysis, since the experimental Φ were higher than unity. All fitting was performed with MAPLE (Maple, Waterloo Maple Inc., Ontario, Canada, www.maplesoft.com).

RESULTS

Preparation of Functional Spin-Labeled TLL Proteins. Eleven TLL single-cysteine mutants were produced in which a selected residue on the surface of the enzyme was replaced with cysteine. The mutation sites were preselected to provide a coverage around the surface of the molecule, using TLL X-ray structures for reference (several structures, published

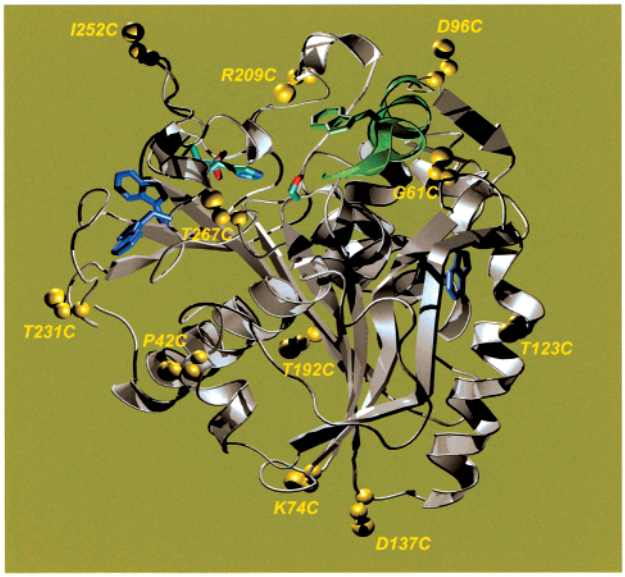

FIGURE 1: Cartoon representation of *T. lanuginosa* lipase (TLL) showing the open conformation (the complexed *n*-dodecyl (C12) phosphonate inhibitor has been omitted in this figure for clarity). The relative positions of all single-point cysteine mutations prepared in TLL are highlighted in yellow (single amino acid codes used). The catalytic triad, consisting of Ser146, His258, and Asp201, is marked in cyan/red. In addition, all four tryptophans in TLL are indicated, and the lid is colored green. The TLL C12 atomic coordinates were kindly provided by Lawson and Brzozowski (*20*). The figure was generated using POV-Ray and VMD (*61*).

as well as nondeposited, of TLL in the open or closed conformation were used). A structure of TLL in the open conformation, complexed with an *n*-dodecyl (C12) phosphonate inhibitor, is shown in Figure 1 [the TLL C12 atomic coordinates were provided by Lawson et al. (*20*)]. This cartoon representation shows the relative positions of all single-cysteine mutations prepared in TLL. Five mutations were placed around the active site and the lid [T267C (Thr267 replaced by cysteine), I252C, R209C, D96C, and G61C]. On the lower third of the molecule a ring of residues was mutated (P42C, T231C, T192C, and T123C), and at the bottom of the enzyme are K74C and D137C, which are placed close together but positioned at the turns of two different loops. Cloning, expression, and purification of the proteins afforded fully active TLL mutants, which in all cases produced one single band of 33 kDa on SDS−PAGE. The tryptophan emission spectra of all TLL mutants were effectively identical to that of the wild-type lipase (*30*).

The spin labeling was performed after prior treatment of the TLL's with DTT to remove premature disulfide bond formation between the introduced cysteine and endogenous cysteine from the fermentation (as confirmed by electrospray MS).[3] Optimal reduction conditions were elaborated which selectively reduced the introduced cysteine but none of the three internal disulfide bridges, which was confirmed by the TLL wild-type control. Spin labeling with the sulfhydryl-specific reagent MTSL (Chart 1) was immediately performed after removal of the DTT. Only negligible amounts of spin label (1−2%) were observed in the wild-type control after labeling, which may be attributed to a small amount of hydrophobically attached spin-label reagent still present after purification (*52*). Table 1 shows the specific hydrolytic activity of the produced TLL mutants, the residual activity after spin labeling, and the degree of spin-label incorporation. As seen in Table 1, the specific hydrolytic activity of the TLL cysteine mutants is comparable to or higher than that of the wild-type lipase, which was 5700 LU/mg under the assay conditions. Furthermore, it can be seen that the spin labeling had no severe effect on the activity of the lipases, although some mutants displayed a decrease of activity. The small but unpredicted increase of activity after labeling seen in some cases (I252C, T267C) was attributed to the reduction of the small fraction of covalent dimers observed in some of the mutants. The variations in spin-label incorporation for the TLL mutants were consistent with the anticipated relative steric accessibility of the mutation sites (*34*) but did not coincide with the variations in the residual specific hydrolytic activity (Table 1). Together, the above results show that neither the mutations nor the spin labeling of TLL significantly perturbed the enzyme activity. This is consistent with previous work in which substitutions of solvent-accessible groups on the surface of proteins, in the cases performed, have been shown to have little effect on protein structure and function (*53*, *54*). Furthermore, nitroxide side chains placed on the surface of a protein should not cause perturbations [molecular volume of ~269 Å compared to ~229 Å for tryptophan (*34*)].

Table 1: Specific Hydrolytic Activity and Degree of Spin-Label Incorporation for TLL Cysteine Mutants[a,b]

variant	specific act.[c] (LU/mg)	residual act.[d] (LU/mg)	spin-label incorporation[e] (mol %)	mutation position
P42C	6210 ± 50	5680 ± 10	21 ± 3	α-helix[f]
G61C	6660 ± 10	3420 ± 10	13 ± 1	β-turn
K74C	7300 ± 110	4960 ± 90	13 ± 2	β-hairpin
D96C	6450 ± 100	3060 ± 240	53 ± 6	loop
T123C	7200 ± 60	3650 ± 10	23 ± 2	α-helix
D137C	7130 ± 300	6540 ± 200	52 ± 8	β-turn
T192C	6710 ± 300	5740 ± 140	8.0 ± 0.9	β-sheet
R209C	7640 ± 10	6520 ± 150	26 ± 3	α-helix
T231C	6360 ± 240	4090 ± 130	52 ± 5	β-hairpin
I252C	5080 ± 230	5340 ± 80	100 ± 12	loop
T267C	3850 ± 160	4660 ± 70	14 ± 2	loop[f]

[a] Measured by pH stat on a 16 mM emulsion of glyceryl tributanoate at pH 7.0 and 25 °C. [b] One lipase unit (LU) equals 1 μmol of released titratable acid per minute. [c] The specific activity of TLL wild type is 5700 LU/mg. [d] Specific activity after spin labeling. [e] Determined by ESR against MTSL standard solutions. Mol %: mole of spin label per mole of protein, in percent. [f] Positioned next to a disulfide bridge.

Spectral Signatures and Correlation with TLL Secondary Structure. CW ESR spectra for the 11 spin-labeled TLL mutants are displayed in Figure 2. The variants are grouped according to low and high spin-label insertion (panels A and B, respectively). All spectra are characteristic of moderately immobilized nitroxides with rotational correlation times, τ_c, of approximately 1 ns (*33*, *55*). This is consistent with rapid internal motion of the nitroxide side chain due to nearly unrestricted bond rotation when attached to the surface of the enzyme. It should be underlined that the mobility of the spin label in the spectra primarily reflects the motion of the nitroxide relative to the protein and not the tumbling motion of the protein itself. In some spectra, a component of isotropically rotating spin label is detectable, as indicated

[3] A small amount of covalent dimers was also detected in some mutants by SDS−PAGE.

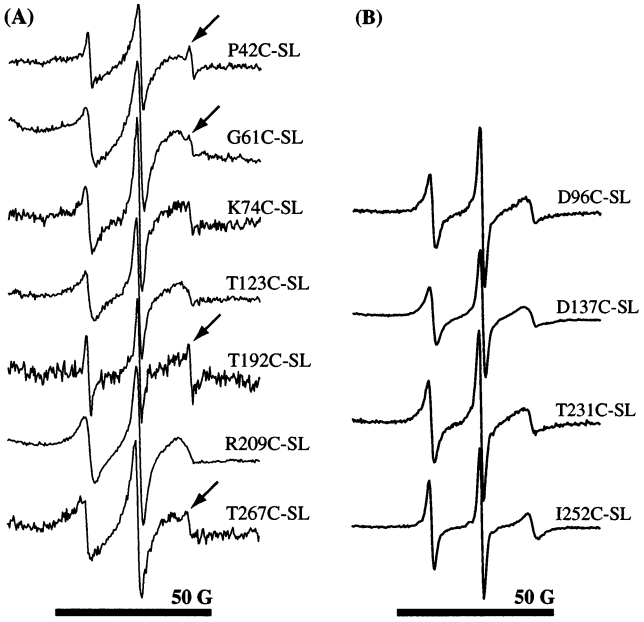

FIGURE 2: First derivative CW ESR spectra recorded in the X-band at 9.75 GHz of site-specifically spin-labeled *T. lanuginosa* lipase cysteine mutants (15−25 μM in 20 mM Na-HEPES, pH 7.0), grouped according to low spin-label insertion (panel A) and high spin-label insertion (panel B). The resonance amplitudes have been normalized with respect to the central $m_{I=0}$ resonance line. The scale of the magnetic field is indicated by a bar, and the identity of the variants is specified in the figure. A small amount (1−2%) of hydrophobically attached spin label is present in some samples, as indicated by arrows.

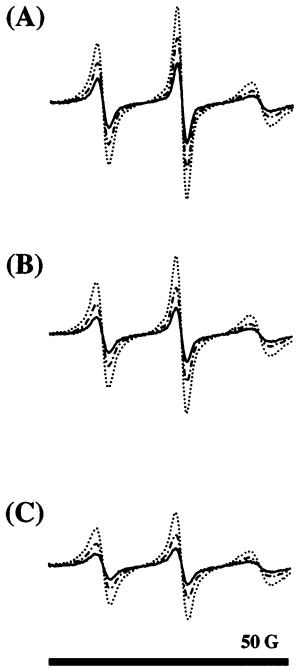

FIGURE 3: First derivative CW ESR spectra recorded in the X-band at 9.75 GHz of the spin-labeled *T. lanuginosa* lipase cysteine mutant I252C-SL (23 μM in 20 mM Na-HEPES, pH 7.0). The spectra are shown for increasing concentrations of Crox ranging from 0 mM (A) to 4.9 mM (B) to 9.8 mM (C) and were recorded at incident microwave powers of 0.6 mW (—), 2.0 mW (− · −), and 6.4 mW (···). The scale of the magnetic field is indicated by a bar.

by the arrows (panel A). This was presumed to originate from a small amount (1−2%) of hydrophobically attached nitroxide still present in some variants (*52*). The spectra in Figure 2A show slightly greater nitroxide immobilization than those in Figure 2B. This is indicative for spin-label side chains on the surface of α-helices or β-sheets (panel A), while the narrower line widths (panel B) are characteristic of spin-label side chains that are attached to highly flexible protein segments, such as hairpin loops [see Table 1 (*55*)]. The greater nitroxide mobility displayed in the spectra in panel B also effected a better signal-to-noise ratio, in combination with the higher degree of spin labeling.

ESR line shapes report on protein backbone dynamics, protein secondary structure, and side chain tertiary contact (*56*). Previous work employing SDSL has shown a correlation between the relative reactivity of cysteines and protein structure, which was also reflected in the relative spin-label mobility displayed in the resulting ESR spectra (*34*). In the present study, the varying degrees of spin-label incorporation for each of the different TLL mutants suggested a dependence of cysteine steric accessibility for the degree of spin-label incorporation. To selectively reduce the cysteine on the surface of TLL prior to spin labeling, it was observed that the reaction time had to be limited. This could potentially lead to less than quantitative labeling in those residues that were more sterically restricted, which may thus react more slowly. Altogether, the different line shapes of the ESR spectra and the degree of spin-label incorporation in the TLL mutants correlate well with the local structural features near the cysteine mutations. It should be stressed that in the present study we only use qualitative features of the spectra to draw inferences about the relative mobility of the nitroxides in the protein. However, analysis of ESR line shapes by simulation can provide detailed information on several levels of spin-label interaction (the reader is referred to two comprehensive monographs on spin labeling in refs *52* and *57*).

Comparison of the ESR Low-Field Method with Progressive Power Saturation. In the present paper the orientation of TLL on POPG vesicles was studied by employing an ESR technique of spin relaxation enhancement performed at low microwave amplitude ($h_1 < 0.36$ G), together with the water-soluble spin relaxation agent Crox. The accuracy of this low-field method was evaluated by comparison with the established method of progressive power saturation. Power saturation measurements were performed by acquiring CW ESR spectra over the full power-saturation range ($h_1 = 0.02-1.6$ G) using a high-field dielectric resonator. This was done on samples of one of the spin-labeled mutants (I252C-SL) containing varying concentrations of Crox. In Figure 3, unsaturated first derivative CW ESR spectra are shown for I252C-SL with increasing incident microwave power and with increasing concentrations of Crox. The power dependence of the central line peak to peak height is seen. It is also apparent that increasing concentrations of the spin relaxation agent caused a major decrease in the signal height as well as a broadening of the line widths. The second integrals of the ESR spectra were confirmed to be independent of the concentration of Crox at low incident power (data not shown).

For each data set, the full range of data points (shown in Figure 4) was fit by nonlinear least-squares regression analysis to eq 1, where P_2, c, and ϵ were allowed to vary, which yielded power saturation rollover curves (*36*). The curves display classical saturation behavior in that the signal

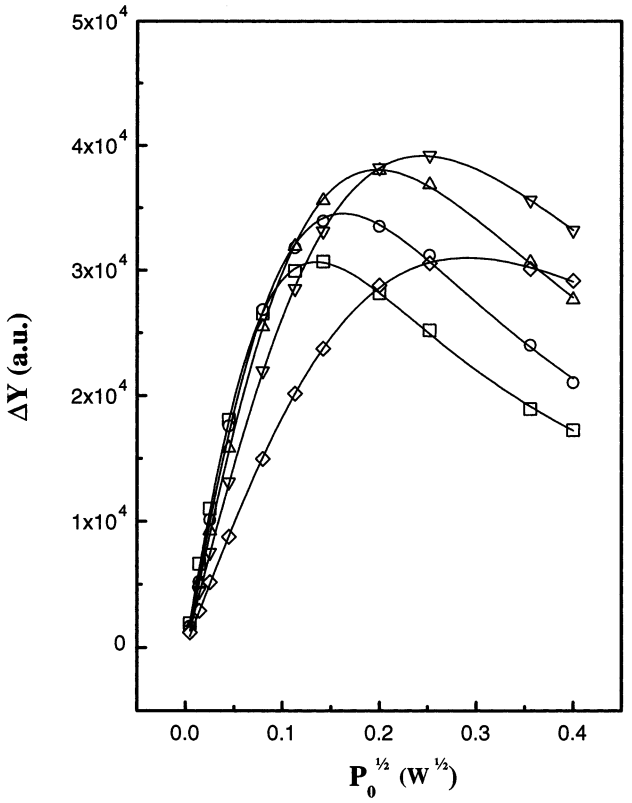

FIGURE 4: Power saturation rollover curves for the spin-labeled *T. lanuginosa* lipase cysteine mutant I252C-SL (23 μM in 20 mM Na-HEPES, pH 7.0) in the absence and presence of Crox. The curves show the peak to peak height of the central line in the first derivative ESR spectrum (ΔY) as a function of incident microwave power for I252C-SL together with Crox at the following concentrations: 0 mM (□), 1.25 mM (○), 2.50 mM (△), 4.95 mM (▽), and 9.80 mM (◇). The data points were fitted by nonlinear least-squares regression to eq 1, as indicated by the solid lines. The incident microwave power range used equals a microwave amplitude, h_1, of 0.02−1.6 G.

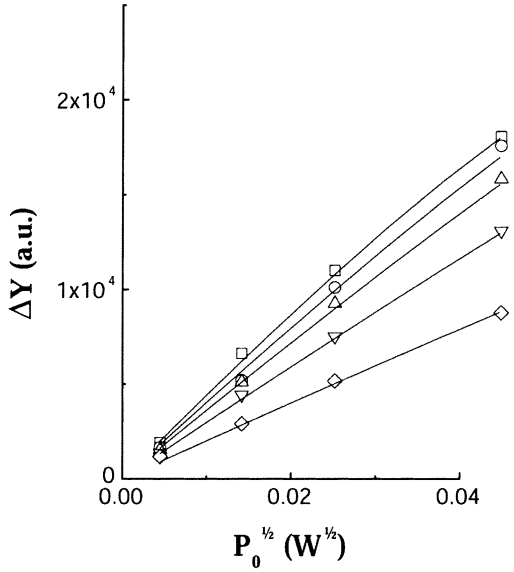

FIGURE 5: An enlarged segment of the rollover curves in Figure 4, displaying the linear range of the curves at low incident microwave power.

Table 2: Values of P_2, ϵ, and c for I252C-SL Obtained from Power Saturation Rollover Curves

[Crox] (mM)	P_2 (W)[a]	ϵ[a]	c[a]	c[b]
0	0.022 ± 0.001	1.10 ± 0.02	442900 ± 4000	403300 ± 15000
1.25	0.039 ± 0.004	1.24 ± 0.06	403600 ± 5500	394700 ± 6700
2.49	0.062 ± 0.003	1.30 ± 0.04	361900 ± 2200	355000 ± 5400
4.95	0.108 ± 0.006	1.40 ± 0.05	297100 ± 120	291300 ± 4500
9.80	0.130 ± 0.02	1.28 ± 0.10	200700 ± 130	193400 ± 4200

[a] Obtained by nonlinear least-squares regression analysis of the power saturation data to eq 1. [b] Obtained by a linear least-squares fit to eq 1a of data points in the linear range of the rollover curves, according to the low-field method.

intensity first rises to a maximum, P_{max}, with increasing incident power, and then decreases. Increased concentrations of Crox monotonically decreased the signal intensity in the low incident power region. However, at saturating power, ΔY was seen to depend on the Crox concentration in a more complex manner than in the linear region. Finally, it is seen from Figure 4 that fitting the values to the model represented by eq 1 gave an accurate description of the data sets (*36*, *39*). Figure 5 shows an enlarged segment of the power saturation rollover curves, displaying the linear range of the curves at low incident microwave power. The values of P_2, ϵ, and c obtained from the nonlinear regression analysis of the data points are listed in Table 2. In addition, proportionality constants, c, obtained by a linear least-squares fit of the first four data points in the curves are shown. As seen, the values of the slopes were approximately independent of the method of deriving them.

The parameters P_2, ϵ, and c obtained at the different Crox concentrations were used for comparing the linear low-field method of spin relaxation analysis with the power saturation method. In Figure 6 the quantitative effect of Crox on spin relaxation for I252C-SL is displayed according to the equations (eqs 5 and 6, respectively) and as analyzed by the different methods. Panel A shows the difference in the maximum of the rollover curves, ΔP_{max}, as a function of Crox concentration, and panel B shows the corresponding dependence for the difference in the inverse square root of the slope, $\Delta c^{-1/2}$. The solid lines represent the best linear least-squares fit to the data. In both cases, it is seen that the data points are linearly related to Crox concentration. The slopes in Figure 6 reflect the relative nitroxide accessibility to Crox and were $6.9 \times 10^{-3} \pm 0.5 \times 10^{-3}$ W/mM (panel A) and $7.5 \times 10^{-5} \pm 0.2 \times 10^{-5}$ $W^{1/4}$/mM (panel B), respectively. The error in the individual data points was small for the low-power method: between 1% and 5% (panel B).

The parameter observed using the low-field method is the spin−spin relaxation rate, R_2, at subsaturating microwave amplitudes, h_1, which makes the method applicable also on standard ESR equipment with low conversion efficiency between incident power and microwave amplitude. It has been shown that the spectral line widths broaden monotonically and that the spin−spin relaxation time (T_{2e}) decreases with increasing concentration of spin relaxation agent (*58*). However, it has previously been assumed that the effect on R_2 was too small to measure since the T_{2e} relaxation time is short on the time scale of a molecular collision. Nevertheless, the results presented in the present paper showed that it is indeed detectable in a quantitative manner. The presented results correlate well with the proposed theories (*36*, *39*), and the validity of using the linear low-field approach within this system is evident from the experimental data. It was

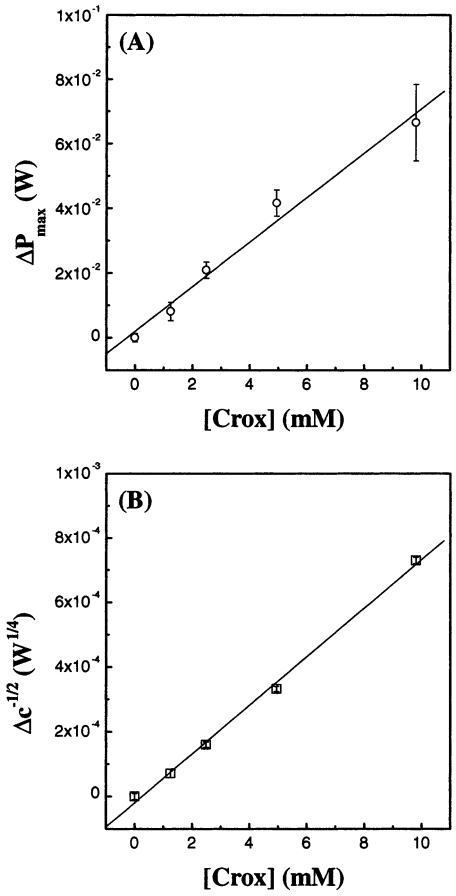

FIGURE 6: Effect of Crox concentration on spin relaxation enhancement for the spin-labeled *T. lanuginosa* lipase cysteine mutant I252C-SL. Panel A shows the dependence of ΔP_{max} on the concentration of Crox, as derived by progressive power saturation analysis. Panel B shows the corresponding dependence of $\Delta c^{-1/2}$ on the concentration of Crox, as obtained by the low-field method. The solid line represents a linear least-squares fit to the data points. The errors in ΔP_{max} and $\Delta c^{-1/2}$ are indicated by error bars (the error in $\Delta c^{-1/2}$ was small: 1−5%).

shown that the maximum of the rollover curve and the inverse square root of the slope, at subsaturating microwave amplitudes, gave the same result regarding spin relaxation enhancement and, thus, specifically regarding the local concentration of Crox.

Determination of TLL Exposure Factors on POPG SUV. The interfacial orientation of TLL on POPG SUV, to which TLL previously has been shown to bind in a catalytically active conformation (*30*), was investigated by employing the ESR low-field method. Subsaturating ESR measurements were performed at low incident microwave amplitude (h_1 < 0.36 G) using a standard resonator. Crox was employed to probe the accessibility to the aqueous phase of the nitroxides on the surface of the protein. POPG SUV were prepared and analyzed by dynamic light scattering, which revealed a narrow vesicle size distribution with a mean of 57 nm and a polydispersity of 0.15. It was confirmed that the vesicle integrity was unchanged after titration with TLL wild-type enzyme and mutants or with Crox in millimolar concentrations (data not shown). The ability of Crox to relax the nitroxide of each of the spin-labeled TLL variants was quantified by acquiring the CW ESR spectra as a function of incident microwave power. The spectra were recorded in the absence and presence of 9.8 mM Crox for the enzyme

Table 3: Exposure Factors, Φ, on POPG SUV and Stern−Volmer Quenching Constants, K_{SV}, for the Quenching of Fluorescence in Dansyl-Labeled POPG SUV for Spin-Labeled TLL Cysteine Mutants

variant	Φ[a]	K_{SV} (M^{-1})[b]
P42C-SL	0.85 ± 0.24	1420 ± 420
G61C-SL	0.06 ± 0.15	2730 ± 310
K74C-SL	0.34 ± 0.30	2320 ± 650
D96C-SL	0.88 ± 0.04	690 ± 190
T123C-SL	0.79 ± 0.14	1380 ± 380
D137C-SL	1.16 ± 0.15	620 ± 190
T192C-SL	0.82 ± 0.24	3100 ± 470
R209C-SL	0.56 ± 0.11	1400 ± 210
T231C-SL	1.03 ± 0.03	640 ± 180
I252C-SL	1.37 ± 0.07	290 ± 80
T267C-SL	0.23 ± 0.14	2550 ± 430

[a] Calculated according to eq 7 on ESR data obtained by the low-field method. [b] Normalized according to TLL spin-label incorporation.

in buffer or bound to the POPG vesicles. For each variant data set, the dependence on incident power of the peak to peak height of the central line in the first derivative ESR spectra was analyzed by linear least-squares regression of the data points to eq 1a. The difference in the inverse square root of the slope, $\Delta c^{-1/2}$, upon addition of Crox was determined for each variant with and without vesicles. As shown in the previous section, the quantity $\Delta c^{-1/2}$ is directly proportional to the local Crox concentration at the spin probe moiety (eq 6), and the presence of a membrane reduces this concentration. The values of $\Delta c^{-1/2}$ obtained in the presence and absence of vesicles were used to calculate the exposure factors, Φ (eq 7). Values of Φ are shown in Table 3. The spin-labeled TLL mutant I252C-SL has the nitroxide placed opposite to the lid but far away from the active site nucleophile Ser146, as does T231C-SL positioned below I252C-SL. Together with these locations, the nitroxide in D137C-SL at the "bottom" face of TLL opposite the active site, displayed the largest value of Φ, which indicates maximum exposure to Crox and the aqueous phase. Ideally, one would expect values close to unity for these exposed positions, but they were slightly higher. At the other extreme were G61C-SL and T267-SL with values close to zero: 0.06 and 0.23, respectively. Thus, the nitroxides at these positions were shielded from Crox relaxation by the lipid membrane. As expected, these spin labels were also the closest to the active site nucleophile, Ser146, of all positions tested. The rest of the spin-labeled mutants displayed intermediate values of Φ. However, there was one exception to the tendency of shielding around the active site. K74C-SL has a value of Φ that indicates less than medium exposure to Crox. This is not easily rationalized, as the nitroxide in K74C-SL is positioned almost directly opposite the active site in TLL and would be expected to show high exposure.

Determination of Stern−Volmer Quenching Constants and Comparison of Data. As an independent technique, fluorescence spectroscopy was employed to measure the quenching of fluorescence in dansyl-labeled POPG vesicles, as exerted by the nitroxide of the interfacially bound spin-labeled proteins (*47*, *48*). In contrast to the ESR method, which measures the interaction between the spin labels and the aqueous phase, the fluorescence method measures the direct interaction between the spin labels and the lipid bilayer. The change in the dansyl emission of the vesicles was first monitored with the unlabeled TLL mutants, to distinguish

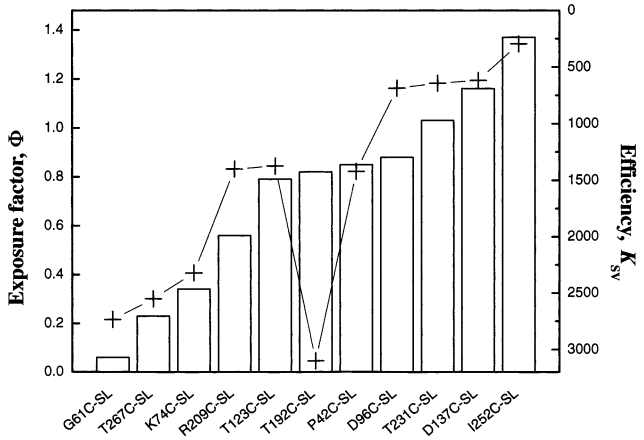

FIGURE 7: Correlation between the exposure factor Φ (bars) and the quenching efficiency K_{SV} (crosses) for the different spin-labeled TLL cysteine mutants. Error bars are omitted for clarity and are listed in Table 3.

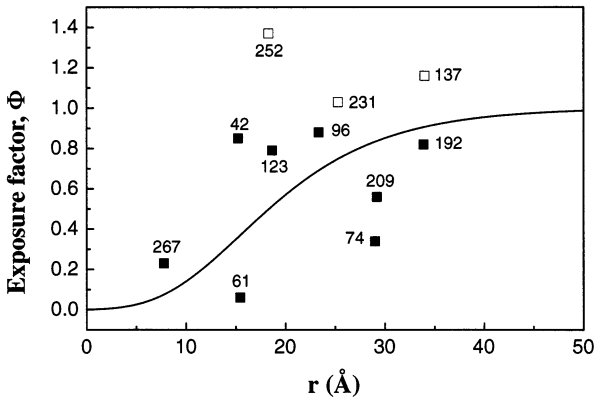

FIGURE 8: Theoretical exposure factors Φ(*r*) and regression analysis of the TLL−membrane orientation. The solid line represents values of Φ calculated as a function of the distance (*r*) from the spin label to the membrane (eq 10). Experimental Φ are shown for the spin labels as a function of the modeled distance from the membrane (■). Corresponding values, as extracted from the modeled structure, are shown for the spin labels excluded from the minimization trials (□).

any contribution of the protein itself from the perturbation of the nitroxide, and subsequently with the spin-labeled mutants. The differences in the resulting Stern−Volmer quenching constants, K_{SV}, were attributed to the direct interaction between the nitroxide and the dansyl fluorophore, and were furthermore normalized according to the degree of spin-label incorporation in the spin-labeled proteins. Table 3 shows the quenching constants for the spin-labeled variants, where a high value signifies high quenching efficiency. Low quenching efficiency was displayed by I252C-SL, D137C-SL, and T231C-SL, which again suggested that these nitroxides were distant from the lipid membrane. On the other hand, high quenching efficiency was seen for G61C-SL and T267C-SL, which was also in agreement with the ESR data. Interestingly, the low exposure to Crox that was measured for K74C-SL was corroborated by the high value of K_{SV} obtained, suggesting that there may exist a second, low-affinity, distinct binding mode for TLL on the vesicles. The rest of the spin-labeled mutants displayed K_{SV}'s of intermediate magnitude, with the exception of T192C-SL, which showed an unexpectedly high value. The correlation between the exposure factors (Φ) and the quenching constants (K_{SV}) is illustrated in Figure 7. It is evident that the two methods agreed well in describing the position of each nitroxide with respect to the lipid membrane, with one curious exception. Two distinct groups of the spin-labeled mutants can now be distinguished: one with low Φ and high K_{SV} and another with high Φ and low K_{SV}, corresponding to nitroxides proximal and distant to the lipid membrane, respectively. The other spin-labeled mutants displayed intermediate values of Φ and K_{SV}.

Calculation of Electrostatic Potential-Modulated Crox Concentrations and Regression Analysis of TLL−Membrane Orientation. The value of the exposure factor, Φ, reflects the effective local concentration of the spin relaxant, Crox, at the spin-label moiety of the membrane-associated SL-TLL's. The basis for understanding the exposure factors is that the surface of the charged POPG vesicles has a negative electrostatic potential, which repels the anionic Crox. This results in a reduced concentration of Crox near the membrane in relation to its bulk concentration. In the present paper, the molar concentration of Crox, due to the electrostatic potential generated by the membrane, was calculated as a function of the normal distance *r* from the membrane (eqs 8 and 9). Theoretical exposure factors Φ(*r*) were calculated as $\Phi(r) = C_{Crox}(r)/C_{Crox}(\infty)$, in analogy to eq 7 (*36*). The solid line in Figure 8 shows the theoretical exposure factor Φ as a function of the distance between the spin label and the membrane (*r*). The calculations are based on the assumption that the membrane that contacts the enzyme is a plane of uniform charge density (for a discussion regarding local inhomogeneities of electrostatic potential due to the protein, see ref *36*). A comparison of the theoretical values with the experimentally derived values of Φ allowed the determination of the normal distance between each spin label and the membrane. Together with the TLL open conformation X-ray structure (*20*), the distances were used for a regression analysis of the TLL−membrane orientation (*36*). The open TLL structure was chosen as a model, since it is known that TLL adopts the open conformation when it is bound to the POPG SUV (*30*). Furthermore, the conformational change leading to the interfacial activation of TLL involves the rotation of a short (approximately 10 amino acid long) α-helix around its two hinge regions. When superimposing the open and the closed X-ray structures of TLL, it can be seen that this conformational change is essentially restricted to the lid (Figure 9). The exposure factors Φ, resulting from the regression analysis, are shown as squares in Figure 8, and the derived structure is shown in Figure 10. Three of the 11 spin labels (at positions D137C, T231C, and I252C) were excluded from the minimizations since they had values of experimental Φ higher than unity. The closed squares in Figure 8 show the experimental Φ as a function of the modeled distance between each spin label and the membrane. In addition, distances for the spin labels that were not included in the minimizations (shown as open squares) were extracted from the final modeled structure. It can be seen that the modeled Φ correlate fairly well with the theoretical values. However, among the modeled positions, two of the three spin labels (at positions K74C, T192C, and R209C) that are located on the back side of TLL display the most substantial deviations from the theoretical values. This is in agreement with the experimental data that indicated less than average distances from the lipid for these spin

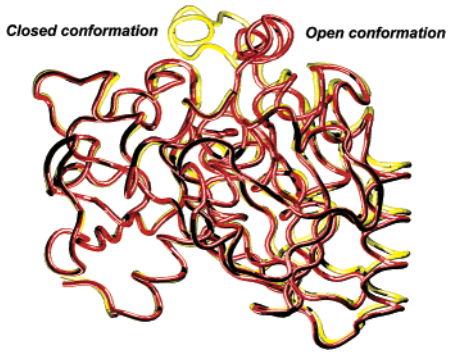

FIGURE 9: Superposition of the Cα backbone of the closed (yellow) and open (red) TLL X-ray structures [accession number 1TIB from the Protein Data Bank (*62*); structure kindly provided by Lawson et al. (*20*)] showing the lid movement in TLL. The figure was generated using POV-Ray and VMD (*61*).

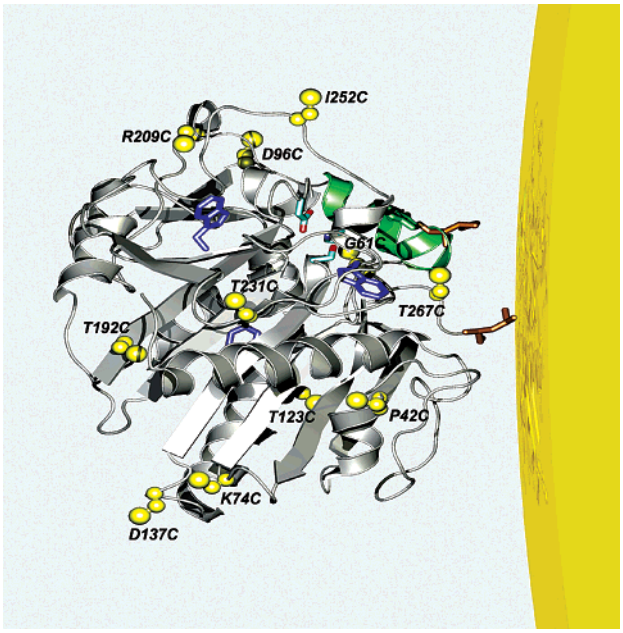

FIGURE 10: Modeled structure for the orientation of *T. lanuginosa* lipase on the surface of a small unilamellar POPG vesicle (yellow), based on the ESR and the fluorescence data obtained in this study. This ribbon representation shows the distance of each spin-labeled cysteine (in yellow) to the membrane (spin labels not shown). The lipase is oriented with the residues G61C and T267C close to the vesicle surface. The proximal part of the open lid (green) is facing the lipid bilayer, together with Ile86 and Leu269 (orange). The TLL C12 atomic coordinates (the C12 phosphonate inhibitor is omitted in this figure for clarity) were kindly provided by Lawson et al. (*20*). The figure was generated using POV-Ray and VMD (*61*).

labels, even though they are positioned far from the active site in TLL. The resulting modeled structure of TLL (Figure 10) shows that the enzyme binds with the spin-labeled residues G61C and T267C close to the membrane. Interestingly, Ile86, which is positioned in the lid of TLL, and the C-terminal Leu269 are seen to be oriented toward the lipid bilayer, suggesting that they might play a role in stabilizing the TLL interfacial binding through hydrophobic interactions with the lipid.

DISCUSSION

Model for the Interfacial Orientation of TLL on POPG SUV. On the basis of the obtained experimental data and the regression analysis, a model for the interfacial orientation of TLL on POPG SUV was proposed (Figure 10). The mutants with the lowest exposure (Φ) to Crox (G61C-SL and T267C-SL) have the nitroxide positioned not only in proximity to the active site area in TLL but also close to the nucleophilic Ser146. Furthermore, the nitroxides at positions T123C, P42C, and D96C, which displayed moderate exposure to Crox, are all located around G61C and T267C. Together, these positions outline a putative contact surface. This approximate plane is somewhat tilted with respect to the lid in TLL and would suggest that the lipid molecules to be hydrolyzed enter the active site from the face where Ser146 is situated. The shape of TLL may be described as a relatively spherical ellipsoid with the dimensions 53 × 48 × 41 Å and an average radius of 23 Å. The regression analysis afforded normal membrane distances for the nitroxides closest to the vesicle surface as follows (Figure 8): 8 Å (T267C-SL), 15 Å (G61C-SL), 15 Å (P42C-SL), 19 Å (T123C-SL), and 23 Å (D96C-SL). The distances obtained indicate that there is no deep penetration of TLL residues into the lipid bilayer. However, the proximal segment of the lid in TLL, and the isoleucine and leucine at positions 86 and 269, would most likely be interacting with the lipid bilayer.

Both spectroscopic techniques used in this study revealed the exposure to the aqueous phase for spin labels on one side of TLL and the proximity to the lipid membrane of two spin labels on another face (positions G61C and T267C). The tilt of the proposed TLL contact surface with respect to the lid is clearly indicated by the obtained experimental data (Φ, K_{SV}) for the diagnostic spin labels at positions P42C, T123C, D96C, and I252C. The orientation of TLL with Ser146 in close proximity to the lipid is intuitively logical, and the entry of substrate molecules to the active site would presumably be aided by the large hydrophobic patch formed by the open lid in conjunction with the exposed active site.

The experimental data indicated that K74C-SL had its nitroxide quite close to the lipid membrane, although this residue is situated opposite to the active site in TLL and would be expected to show high exposure to the aqueous medium. The existence of a second, remote binding site in TLL is not easily rationalized, yet there is experimental evidence thereof (*59*). A suspension of POPG SUV, in which half of the population was labeled with the donor-fluorophore NBD and the other half with the acceptor-fluorophore rhodamine (Rh), displayed no fluorescence resonance energy transfer (FRET) between the vesicles. However, when TLL was added (lipid/enzyme 500:1), there was a strong increase in FRET. The experiments were conducted by adding TLL to the vesicle mixture, or by adding TLL to one population (NBD), and then adding the second population (Rh), which afforded the same result. The aggregation was reversible, since the FRET disappeared upon addition of an excess of unlabeled vesicles (*59*). Combined, these results indicate that TLL binds with high affinity to POPG SUV through the active site surrounding domain (presumably the catalytically active mode) and that another part of the enzyme is responsible for the vesicle aggregation by low-affinity binding to another POPG vesicle.

A second binding mode for TLL on the POPG vesicles is possibly also reflected in the exposure factors observed for T192C-SL and R209C-SL, which have their spin label

positioned in a straight vertical line above K74C-SL on the back side of TLL. However, one difficult interpretation remains to be made. The residues K74C-SL and D137C-SL are found quite close to each other in the X-ray structure but display deviating values of K_{SV} and Φ. Consequently, the two-mode model requires the assumption that the side chain of D137C-SL swings away from K74C-SL as TLL binds to the vesicle and the lid opens.

POPG Vesicles as a Model Interface for TLL. A recent study, employing TLL wild-type enzyme and tryptophan mutants, has shown that TLL binds to small unilamellar vesicles (SUV) consisting of POPG in a catalytically competent form and with the lid open. This was demonstrated by a combination of different fluorescence techniques and kinetic measurements (*30*). POPG is a phospholipid, and it is not a substrate for TLL because the anionic phospholipid has a poor affinity for the active site of the bound enzyme (*60*). However, POPG SUV provide a stable diluent interface to which TLL binds and hydrolyzes substrates partitioned at the interface or included into the lipid bilayer of the vesicle (*30*). There are several advantages to using POPG vesicles for studying the binding and the interfacial orientation of TLL. This lipid spontaneously forms interfaces with well-defined composition and organization, and its main phase transition temperature is optimal. On the other hand, triglycerides, the natural substrates for triglyceride lipases, do not generate well-defined aggregates of known surface area (*30*). In addition to the polymorphism and uncontrolled organizational state of the aggregates, product formation would be a further complication in any spectroscopic measurements.

To our knowledge, the present study provides the first experimental evidence of the detailed interfacial orientation at the lipid−water boundary for a triglyceride lipase. Furthermore, these results, which were obtained using phospholipid vesicles, should give some insight into the binding orientation of TLL on triglyceride aggregates. Although POPG has an anionic headgroup, the active site of TLL did come out to be near the membrane surface, giving some validity to the results and conforming with previous reports showing that TLL displays activity when bound to the POPG vesicles (*30*).

Exposure Factors for Docking TLL on Lipid Membranes. The orientation of bee venom phospholipase A_2 on lipid vesicles was recently investigated by means of ESR progressive power saturation and electrostatic potential-modulated spin relaxation (*36*). The authors introduced an exposure factor, Φ, defined as the relative exposure to a water-soluble spin relaxation agent for nitroxides on the surface of an interfacially bound protein. Similarly, direct determinations of relaxation times and correlation times have also been reported (*38*). The advantage with using the exposure factors is that the relative change in spin relaxation in the presence and absence of vesicles is measured for each enzyme separately, thus enabling a direct comparison between the spin-labeled proteins (*36*). It should also be stressed that the intrinsic relaxivities of a nitroxide in two proteins need not be the same (*39*); hence, it is important to use the relative changes as a measure of relaxation enhancement.

Acquired values of Φ are expected to range between 0 and 1, reflecting minimum and maximum exposure to the relaxation agent, respectively (*36*). In the present paper, values slightly larger than unity were seen in some cases, as a result of changes in the ESR signal upon membrane binding. This phenomenon has been observed previously and is thought to stem primarily from altered local dynamics of the spin probe (*36*). Furthermore, the enzyme studied in the present paper is a fairly flexible protein, in which conformational changes leading to the opening of the lid take place upon activation. Structural changes upon binding could release possible geometrical constraints on the spin label, leading to an increase in the ESR signal. Therefore, the determination of exposure factors is optimal for a rigid enzyme (*36*). However, effects of constraint were presumed to be small, since the conformational changes governing the interfacial activation of TLL are essentially limited to the lid, and none of the single-cysteine mutations were placed at the lid region in TLL. Also, the good agreement between the two independent spectroscopic techniques, reflected in the complementary values of Φ and K_{SV}, supports this assumption.

Proposed Interfacial Orientation of TLL. The interfacial orientation proposed in the present paper is in agreement with the fluorescence data presented by Cajal, Alsina and co-workers, in which a catalytically competent form of TLL was found to bind with the lid open and partially buried into the lipid bilayer of the anionic POPG vesicles. It is also consistent with the lipase binding with positively charged residues (Lys24, Arg81, Arg84) facing the negatively charged lipid surface, as predicted (*30*).

Recently, Brzozowski and co-workers presented five new crystal structures of TLL as derived from a systematic crystallographic study (*32*). A model for the activation and mechanism of the lid opening was proposed, in which a low activity, activated, and full activity conformation sequence for TLL was presented. According to the crystal structures, the lid opening is mediated through an isomerization of a disulfide bridge (Cys268−Cys22). This was thought to coincide with a flip of the adjacent Arg84, and these interacting residues were proposed to act as a "negative sensor" as TLL approaches a lipid or a negatively charged surface (*32*). This arginine is close to the contact residues G61C and T267C found in the present study. Thus, the proposed interfacial orientation of TLL on the POPG vesicles conforms well also with the above model.

In conclusion, the binding orientation of *T. lanuginosa* lipase on small unilamellar phospholipid vesicles has been studied by employing site-directed spin labeling in combination with ESR relaxation spectroscopy and fluorescence spectroscopy techniques. Through the obtained results, an interfacial orientation of TLL was found, in which the proximal part of the open lid is interacting with the lipid, exposing the active site to the membrane. The production of 11 site-selectively spin-labeled single-cysteine mutants, each with a defined label position at the enzyme surface, has enabled the study of spin-label interactions with both the aqueous phase and the lipid phase, at the water−lipid interface.

ACKNOWLEDGMENT

Fruitful discussions with Dr. Bruce H. Robinson are gratefully acknowledged. We thank Dr. Yolanda Cajal for kindly sharing unpublished experimental data as a personal

communication in the present paper. Dr. Flemming Y. Hansen is thanked for assistance with the theoretical calculations.

REFERENCES

1. Klibanov, A. M. (1989) *Trends Biochem. Sci. 14*, 141−144.
2. Björkling, F., Godtfredsen, S. E., and Kirk, O. (1991) *Trends Biotechnol. 9*, 360−363.
3. Dordick, J. S. (1992) *Trends Biotechnol. 10*, 287−293.
4. Faber, K., and Franssen, M. C. R. (1993) *Trends Biotechnol. 11*, 461−470.
5. Vulfson, E. N. (1993) *Trends Food Sci. Technol. 4*, 209−215.
6. Sarney, D. B., and Vulfson, E. N. (1995) *Trends Biotechnol. 13*, 164−172.
7. Svendsen, A., Clausen, I. G., Patkar, S. A., Borch, K., and Thellersen, M. (1997) *Methods Enzymol. 284*, 317−340.
8. Sarda, L., and Desnuelle, P. (1958) *Biochim. Biophys. Acta 30*, 513−521.
9. Jutila, A., Zhu, K., Patkar, S. A., Vind, J., Svendsen, A., and Kinnunen, P. K. J. (2000) *Biophys. J. 78*, 1634−1642.
10. Zhu, K., Jutila, A., Tuominen, E. K. J., and Kinnunen, P. K. J. (2001) *Protein Sci. 10*, 339−351.
11. Brady, L., Brzozowski, A. M., Derewenda, Z. S., Dodson, E., Dodson, G., Tolley, S., Turkenburg, J. P., Christiansen, L., Huge-Jensen, B., Norskov, L., Thim, L., and Menge, U. (1990) *Nature 343*, 767−770.
12. Winkler, F. K., D'Arcy, A., and Hunziker, W. (1990) *Nature 343*, 771−774.
13. Schrag, J. D., Li, Y., Wu, S., and Cygler, M. (1991) *Nature 351*, 761−764.
14. Grochulski, P., Li, Y. G., Schrag, J. D., Bouthillier, F., Smith, P., Harrison, D., Rubin, B., and Cygler, M. (1993) *J. Biol. Chem. 268*, 12843−12847.
15. Noble, M. E. M., Cleasby, A., Johnson, L. N., Egmond, M. R., and Frenken, L. G. J. (1993) *FEBS Lett. 331*, 123−128.
16. Lawson, D. M., Brzozowski, A. M., Dodson, G. G., Hubbard, R. E., Huge-Jensen, B., Boel, E., and Derewenda, Z. S. (1994) in *Lipases—their biochemistry, structure and application* (Wolley, P., and Petersen, S., Eds.) pp 77−94, Cambridge University Press, Cambridge.
17. Brzozowski, A. M., Derewenda, U., Derewenda, Z. S., Dodson, G. G., Lawson, D. M., Turkenburg, J. P., Björkling, F., Huge-Jensen, B., Patkar, S. A., and Thim, L. (1991) *Nature 351*, 491−494.
18. van Tilbeurgh, H., Egloff, M. P., Martinez, C., Rugani, N., Verger, R., and Cambillau, C. (1993) *Nature 362*, 814−820.
19. Grochulski, P., Bouthillier, F., Kazlauskas, R. J., Serreqi, A. N., Schrag, J. D., Ziomek, E., and Cygler, M. (1994) *Biochemistry 33*, 3494−3500.
20. Lawson, D. M., Brzozowski, A. M., Rety, S., Verma, C., and Dodson, G. G. (1994) *Protein Eng. 7*, 543−550.
21. Hermoso, J., Pignol, D., Penel, S., Roth, M., Chapus, C., and Fontecilla-Camps, J. C. (1997) *EMBO J. 16*, 5531−5536.
22. Derewenda, Z. S. (1994) *Adv. Protein Chem. 45*, 1−52.
23. Schrag, J. D., and Cygler, M. (1997) *Methods Enzymol. 284*, 85−107.
24. Schmid, R. D., and Verger, R. (1998) *Angew. Chem., Int. Ed. 37*, 1609−1633.
25. Nardini, M., and Dijkstra, B. W. (1999) *Curr. Opin. Struct. Biol. 9*, 732−737.
26. Ollis, D. L., Cheah, E., Cygler, M., Dijkstra, B., Frolow, F., Franken, S. M., Harel, M., Remington, S. J., Silman, I., Schrag, J., Sussman, J. L., Verschueren, K. H. G., and Goldman, A. (1992) *Protein Eng. 5*, 197−211.
27. Derewenda, U., Brzozowski, A. M., Lawson, D. M., and Derewenda, Z. S. (1992) *Biochemistry 31*, 1532−1541.
28. Grochulski, P., Li, Y., Schrag, J. D., and Cygler, M. (1994) *Protein Sci. 3*, 82−91.
29. Derewenda, Z. S. (1995) *Nat. Struct. Biol. 2*, 347−349.
30. Cajal, Y., Svendsen, A., Girona, V., Patkar, S. A., and Alsina, M. A. (2000) *Biochemistry 39*, 413−423.
31. Martinelle, M., Holmquist, M., and Hult, K. (1995) *Biochim. Biophys. Acta 1258*, 272−276.
32. Brzozowski, A. M., Savage, H., Verma, C. S., Turkenburg, J. P., Lawson, D. M., Svendsen, A., and Patkar, S. (2000) *Biochemistry 39*, 15071−15082.
33. Hubbell, W. L., Cafiso, D. S., and Altenbach, C. (2000) *Nat. Struct. Biol. 7*, 735−739.
34. Todd, A. P., Cong, J. P., Levinthal, F., Levinthal, C., and Hubbell, W. L. (1989) *Proteins: Struct., Funct., Genet. 6*, 294−305.
35. Altenbach, C., Marti, T., Khorana, H. G., and Hubbell, W. L. (1990) *Science 248*, 1088−1092.
36. Lin, Y., Nielsen, R., Murray, D., Hubbell, W. L., Mailer, C., Robinson, B. H., and Gelb, M. H. (1998) *Science 279*, 1925−1929.
37. Hung, S. C., Wang, W., Chan, S. I., and Chen, H. M. (1999) *Biophys. J. 77*, 3120−3133.
38. Kostrzewa, A., Pali, T., Froncisz, W., and Marsh, D. (2000) *Biochemistry 39*, 6066−6074.
39. Haas, D. A., Mailer, C., and Robinson, B. H. (1993) *Biophys. J. 64*, 594−604.
40. Bailar, J. C., and Jones, E. M. (1939) *Inorg. Synth. 1*, 35−38.
41. Christensen, T., Woeldike, H., Boel, E., Mortensen, S. B., Hjortshoej, K., Thim, L., and Hansen, M. T. (1988) *Biotechnology 6*, 1419−1422.
42. Pace, C. N., Vajdos, F., Fee, L., Grimsley, G., and Gray, T. (1995) *Protein Sci. 4*, 2411−2423.
43. Ellman, G. L. (1959) *Arch. Biochem. Biophys. 82*, 70−77.
44. Briggs, R. G., and Fee, J. A. (1978) *Biochim. Biophys. Acta 537*, 100−109.
45. Pantoliano, M. W., Whitlow, M., Wood, J. F., Dodd, S. W., Hardman, K. D., Rollence, M. L., and Bryan, P. N. (1989) *Biochemistry 28*, 7205−7213.
46. Poole, C. P., Jr. (1967) in *Electron Spin Resonance: A Comprehensive Treatise on Experimental Techniques*, Interscience Publishers, New York.
47. Lakowicz, J. R. (1999) in *Principles of Fluorescence Spectroscopy*, 2nd ed., Plenum Press, New York.
48. Abel, E., Maguire, G. E. M., Murillo, O., Suzuki, I., De Wall, S. L., and Gokel, G. W. (1999) *J. Am. Chem. Soc. 121*, 9043−9052.
49. Pake, G. E., and Tuttle, T. R., Jr. (1959) *Phys. Rev. 3*, 423−425.
50. Altenbach, C., Flitsch, S. L., Khorana, H. G., and Hubbell, W. L. (1989) *Biochemistry 28*, 7806−7812.
51. Lakshminarayanaiah, N. (1984) in *Equations of Membrane Biophysics*, Academic Press, Orlando, FL.
52. Berliner, L. J. (1979) in *Spin Labeling: Theory and Applications*, Vol. II, pp 296−299, Academic Press, New York.
53. Alber, T., Sun, D. P., Nye, J. A., Muchmore, D. C., and Matthews, B. W. (1987) *Biochemistry 26*, 3754−3758.
54. Reidhaar-Olson, J. F., and Sauer, R. T. (1988) *Science 241*, 53−57.
55. Merianos, H. J., Cadieux, N., Lin, C. H., Kadner, R. J., and Cafiso, D. S. (2000) *Nat. Struct. Biol. 7*, 205−209.
56. Hubbell, W. L., Gross, A., Langen, R., and Lietzow, M. A. (1998) *Curr. Opin. Struct. Biol. 8*, 649−656.
57. Berliner, L. J. (1976) in *Spin Labeling: Theory and Applications*, Academic Press, New York.
58. Robinson, B. H., Mailer, C., and Reese, A. W. (1999) *J. Magn. Reson. 138*, 199−209.
59. Cajal, Y. (2000) personal communication.
60. Berg, O. G., Cajal, Y., Butterfoss, G. L., Grey, R. L., Alsina, M. A., Yu, B. Z., and Jain, M. K. (1998) *Biochemistry 37*, 6615−6627.
61. Humphrey, W., Dalke, A., and Schulten, K. (1996) *J. Mol. Graphics 14.1*, 33−38.
62. Berman, H. M., Westbrook, J., Feng, Z., Gilliland, G., Bhat, T. N., Weissig, H., Shindyalov, I. N., and Bourne, P. E. (2000) *Nucleic Acids Res.*, 235−242.

BI020158R